

First Demonstration of Net-1.6-Tbps 4 λ -WDM in 150-GHz-Grid IM/DD Transmission with a Single DAC/channel and Advanced DSP for Intra-Datacenter-Interconnects

An Yan¹, Guoqiang Li¹, Sizhe Xing¹, Yongzhu Hu¹, Wangwei Shen¹, Ziwei Li¹, Chao Shen¹, Jianyang Shi¹, Xi Xiao^{2,3}, Zhixue He³, Nan Chi^{1,3} and Junwen Zhang^{1,3*}

¹Key Laboratory of EMW Information (MoE), Fudan University, Shanghai 200433, China

²National Information Optoelectronics Innovation Center, CICT, Wuhan 430070, China

³Peng Cheng Laboratory, Shenzhen, 518057, China

Corresponding Author: *junwenzhang@fudan.edu.cn

Abstract: For the first time, we experimentally demonstrate net-400-Gb/s/lane 150-GHz-spaced 4 λ -WDM transmission over 0.5-km SSMF in C-band for intra-datacenter-interconnects based on 128-GBaud probabilistically shaped PAM-20, using a single DAC per channel and driver-free, high-bandwidth TFLN modulators. © 2024 The Author(s)

1. Introduction

The recent growing demand for data-center traffic is driven by the rapid spread and massive use of cloud and social media services. A huge number of applications such as social networking and video streaming are supported by Ethernet, which is economically deployed and applied to intra- and inter-datacenter networks. Nowadays Ethernet has already been completed standardization up to 400-GbE at 100-Gb/s per channel with cost-effective intensity modulation and direct detection (IM/DD) schemes [1]. The next-generation Ethernet will require 200 G/lane and even 400 G/lane to achieve 800-GbE and even 1.6-TbE. At present, the 800G multi-source agreement (MSA) has officially announced specifications for 200 G/lane systems [2]. To increase the single-carrier capacity towards 400 Gb/s, it's necessary to transmit high symbol-rate signals, or adopt high-order pulse amplitude modulation (PAM) formats within limited symbol-rate. While the latter approach may result in increased power demands, it is crucial to deliberate higher-order modulation schemes, which are preferred for future 1.6-TbE systems employing wavelength division multiplexing (WDM) due to their enhanced spectral efficiency.

To achieve the net data rate of 400-Gb/s/lane towards the future 1.6-TbE, various system configurations have been utilized in recent reports, as depicted in Fig. 1 [3]–[10]. For example, by employing an optimized digital-band-interleaved digital-to-analog converter (DAC) based on three sub-DAC channels, the authors in [3] experimentally transmit 200-GBaud probabilistically shaped (PS) PAM16 and achieve a net data-rate of 485.5-Gb/s. Another work demonstrates the transmission of 180-GBaud PAM-8 signals (net 450-Gb/s) using only a single DAC channel [8]. Nonetheless, all preceding reports of achieving a 400-Gb/s/lane net bitrate are restricted to single-carrier transmission and lacks experimental validation in the context of WDM. An overview of the recent high-speed WDM IM/DD transmission records is depicted in Fig. 1 (b) [11]–[15]. In [13] and [14], the authors demonstrate 1.6T eight-channel IM/DD optical transmission, which is not spectral-efficient and requires the utilization of eight wavelengths. Another work achieves net 4 \times 500Gb/s IM/DD transmission based on interleaved polarization division multiplexing, which employs eight wavelengths indeed [15]. For the consideration of optical bandwidth efficiency, achieving net 400-Gbps/ λ in potentially 150-GHz-bandwidth is of great interest for future 1.6TbE.

For the first time, this study successfully presents an experimental demonstration of 4 λ -WDM transmission of 1.61-Tbps in C-band, with a per-lane net bitrate exceeding 400 Gb/s in 150-GHz-grid over 0.5-km SSMF for intra-datacenter interconnects. Entropy optimization is applied based on the PS-PAM-20 signals. It is worth noting that there is no driver or trans-impedance amplifier (TIA) used for electrical amplification in both Tx and Rs side. In addition, only single DAC per channel is used for signal generation and directly drives the high-speed thin film lithium niobate (TFLN) modulator on the Tx side.

2. Experimental Setup

Fig. 2 depicts the IM/DD transmission setup. In the transmitter DSP, the mapped symbols are pre-distorted based on a non-linear lookup table (LUT) with a 1-symbol memory length [16]. After that, the symbols are resampled to 2

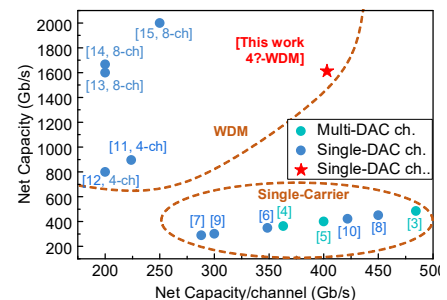


Fig. 1. Net capacity vs net capacity/lane for recent record IM/DD experiments.

samples/symbol (sps) and pulse-shaped by a root-raised-cosine (RRC) filter. Following the linear pre-equalization, the symbols are loaded in the memory of an arbitrary waveform generator (AWG, Keysight M8199B).

At the transmitter side, four distinct WDM channels are established, each employing an external cavity laser (ECL) with a linewidth of 100 kHz. These lasers are operated with 150-GHz frequency grid. Before independent modulation by two thin-film lithium niobate Mach-Zehnder modulators (TFLN-MZM, NOEIC MZ135-LN60), a pair of polarization-maintaining optical couplers (PM-OC) are utilized to enable the segregation of odd channels from even channels. The modulated signals of both odd and even channels are pre-amplified to compensate for power loss before being merged and transmitted through the 0.5-km SSMF. To regulate the received optical power (ROP), a variable optical attenuator (VOA) is strategically inserted before the photodetector (XPDV4121R, with a bandwidth of 100 GHz). The photodetector's current signal is directly sampled by a high-speed oscilloscope (UXR-0594A, 256-GSa/s sample rate).

The offline Rx DSP starts with resampling and timing-recovery. Both linear and nonlinear channel equalization are performed at 2-sps and produce symbol outputs at 1-sps. Then a partial-response post-filter, with impulse response of $1+\alpha D$, is applied to alleviate the noise enhancement in the high frequency components [17]. Following the post filter, a soft- decision BCJR algorithm with two memory taps is used for sequence detection [18]. Finally, we calculate the normalized generalized mutual information (NGMI) based on the log-likelihood ratio (LLR) derived by BCJR demapper [19].

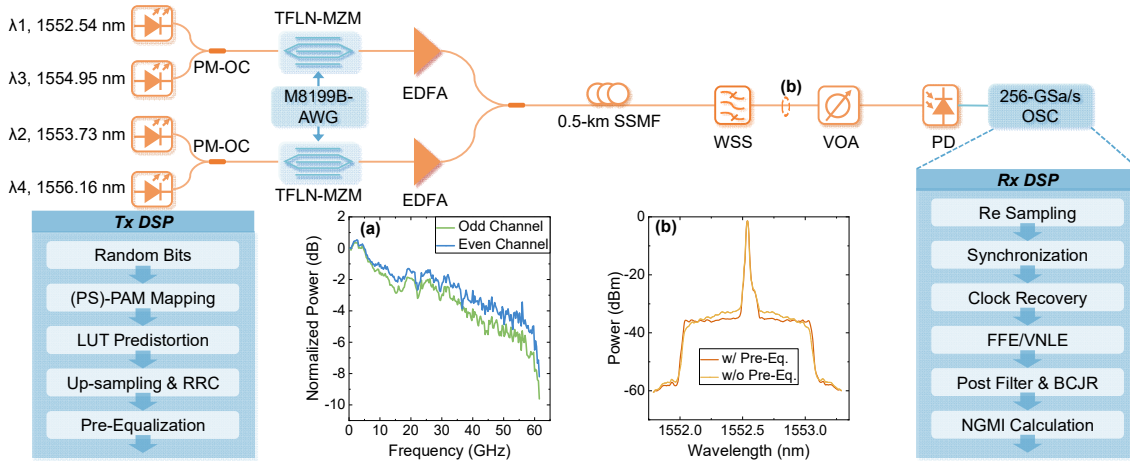


Fig. 2 Experiment setup for the high-order PS-PAM IM/DD transmission system. The inset (a) represents the frequency response of overall system in B2B case, and the inset (b) shows the measured optical spectra after filtering by WSS.

3. Results and Discussions

In this study, we calculate both achievable information rate (AIR) and net bitrates as a metric for data rate. For the evaluation of net bitrates, we consider the concatenated SD+HD FEC coding scheme discussed in [4], and adopt the corresponding NGMI threshold which is associated with the overall code-rate. For each data set, the maximum net bitrate resulted from the achieved highest NGMI threshold is found.

Fig. 3 shows the relationship between NGMI performance and baud-rate for standard PAM-16 signal. We consider linear feedforward equalizer (FFE), and third-order Volterra nonlinear equalizer (VNLE) with/without BCJR partial-response equalization. It is evident that VNLE outperforms linear FFE, primarily attributed to the heightened susceptibility of high-order PAM signals to nonlinear impairments. Furthermore, the BCJR equalization brings a notable improvement in performance, particularly in the scenario of severe bandwidth limitation. The stark decrease in NGMI performance beyond 128-GBaud baud-rate is attributed to the brick-wall filtering of the oscilloscope.

Considering the elevated signal-to-noise ratio (SNR) demands associated with ultra-high-order PAM formats such as PAM-16, we employ the PS method to regulate the source entropy of the PAM signals. Furthermore, we measure the signal from PAM-16, PAM-20, to PAM-22 for data rate optimization. The PAM-20/22 symbols are generated from the standard 512QAM constellations with a pseudo-Gray bit mapping [20]. For PAM-20 and PAM-22 symbols, the coding loss from bit mapping is considered when calculating the net data rate. In Fig. 4, we have systematically varied the entropy of PS-PAM signals to explore the uppermost achievable data rate at 128-GBaud. As shown in Fig. 4, the highest data rate is achieved with PS-PAM-20 at the source entropy of 4.2 bits/symbol. Therefore, we choose PS-PAM20 at 4.2 bits/symbol for the subsequent WDM transmission measurements.

Fig. 5 (a) presents the measured optical spectra of 4 λ -WDM signals. In Fig. 5 (b), we present the measured NGMI as a function of the received optical power (ROP) for PS-PAM20 (4.2bits/symbol) signals in channel 2. As

can be seen, the NGMI threshold 0.8241 (overall code-rate = 0.7684) is achieved [4], resulting in a net data-rate beyond 400Gb/s. Fig. 5(c) illustrates the AIR and net bitrate for all 4WDM channels in both the B2B and fibre-transmission scenarios. Notably, each WDM channel attains a net bitrate exceeding 400 Gb/s (404.2-, 404.2-, 400.5-, 404.2-Gb/s net rates), leading to an aggregate net data rate to 1.61-Tbps.

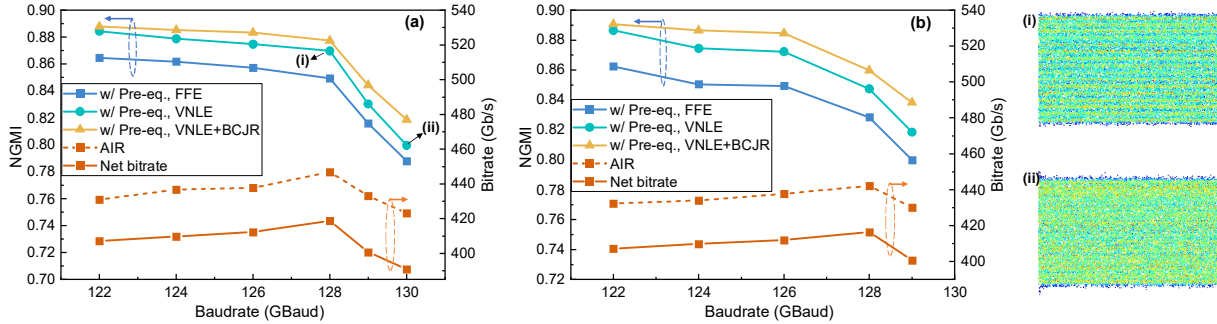


Fig. 3 Single-channel experimental results for standard PAM-16 in (a) B2B, (b) fiber transmission cases.

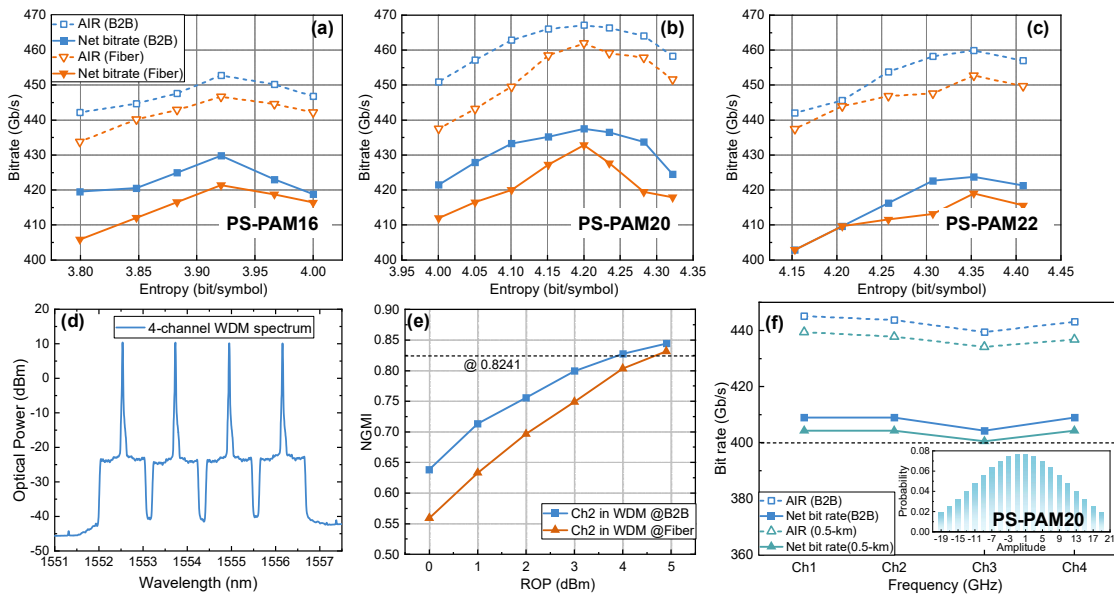


Fig. 4 Single-channel transmission results: the net bitrate and AIR versus source entropy for 128-GBaud (a) PS-PAM16, (b) PS-PAM20 and (c) PS-PAM22 WDM results: (d) The measured optical spectra of 4-channel WDM signals after multiplexing. (e) Measured NGMI as a function of the received optical power for channel-1. (f) The net bitrate and AIR vs channel frequency for 4-channel WDM transmission.

4. Conclusion

We have successfully demonstrated 1.61-Tbps WDM transmission over C-band 0.5-km SSMF using only a single DAC. Each channel carries over 400-Gb/s/carrier net bitrate based on 128-GBaud PS-PAM-20 and the 4 channels of signals are transmitted with 150-GHz-grid spacing. Additionally, no electrical amplifiers are applied at either the transmitter or receiver sides. To the best of our knowledge, this is the first experimental demonstration of net-1.61-Tbps 4 λ -WDM transmission with over net-400-Gb/s/ λ for future 1.6-TbE intra-datacenter interconnects.

Acknowledgment: This work was partly support by the NSFC project (No. 62171137, No. 62235005, No.61925104) Shanghai NSF project (No. 21ZR1408700).

References

- [1] X. Zhou, et al., *J. Light. Technol.*, 38.2, 475–484 (2019).
- [2] P. Dong, et al., in *OFC 2023*, paper M4H.1.
- [3] X. Chen, et al., in *ECOC 2020*, 1-4.
- [4] Q. Hu, et al., *J. Light. Technol.*, 40.10, 3338–3346 (2022)
- [5] H. Yamazaki, et al., *Opt. Exp.*, 27.18, 25544–25550 (2019).
- [6] M. S. Bin Hossain, et al., in *ECOC 2020*, 1-4.
- [7] M. S. Alam, et al., *Photo. Tech. Lett.*, 33.24, 1391–1394 (2021).
- [8] E. Berikaa, et al., *Photo. Tech. Lett.*, 35.15, 850–853 (2023).
- [9] J. Zhang, et al., *Opt. Lett.*, 47.12, 3035–3038 (2022).
- [10] A. Yan, et al., in *ICOCN 2023*, 1-3.
- [11] K. Wang, et al., in *OFC 2020*, paper Th3K.3.
- [12] C. Bluemm et al., *J. Light. Technol.*, 41.12, 3783–3790 (2023).
- [13] T. Rahman et al., in *ECOC 2020*, 1-4.
- [14] P. Xia et al., in *OFC 2023* paper Tu31.6.
- [15] X. Fang et al., in *ECOC 2023*, 1-4.
- [16] Z. He et al., in *ECOC 2020*, 1-4.
- [17] L. Liu et al., in *ECOC 2014*, 1-3.
- [18] D. Che et al., *J. Light. Technol.*, 40.10, 3347–3357 (2022).
- [19] A. Alvarado et al., *J. Light. Technol.*, 33.20, 4338–4352 (2015)
- [20] E. Berikaa et al., *Opt. Lett.* 47.23, 6273–6276 (2022).